Direct visualization of boron dopant distribution and coordination in individual chemical vapor deposition nanocrystalline B-doped diamond grains

Ying-Gang Lu, Stuart Turner, Johan Verbeeck, Stoffel D. Janssens, Patrick Wagner, Ken Haenen, and Gustaaf Van Tendeloo

Citation: Applied Physics Letters **101**, 041907 (2012); doi: 10.1063/1.4738885
View online: http://dx.doi.org/10.1063/1.4738885
View Table of Contents: http://scitation.aip.org/content/aip/journal/apl/101/4?ver=pdfcov
Published by the AIP Publishing

Articles you may be interested in

Low-temperature electrical transport in B-doped ultrananocrystalline diamond film
Appl. Phys. Lett. **104**, 182602 (2014); 10.1063/1.4876130

Local bond length variations in boron-doped nanocrystalline diamond measured by spatially resolved electron energy-loss spectroscopy
Appl. Phys. Lett. **103**, 032105 (2013); 10.1063/1.4813842

Tribological properties of nanocrystalline diamond films deposited by hot filament chemical vapor deposition
AIP Advances **2**, 032164 (2012); 10.1063/1.4751272

Controllable chemical vapor deposition of large area uniform nanocrystalline graphene directly on silicon dioxide
J. Appl. Phys. **111**, 044103 (2012); 10.1063/1.3686135

Ultrananocrystalline diamond film deposition by direct-current plasma assisted chemical vapor deposition using hydrogen-rich precursor gas in the absence of the positive column
J. Appl. Phys. **109**, 023303 (2011); 10.1063/1.3533764

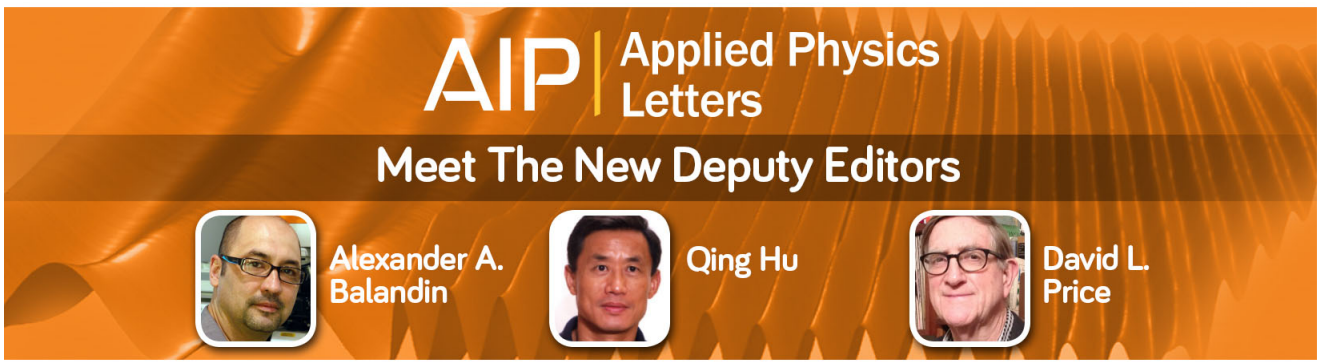

This article is copyrighted as indicated in the article. Reuse of AIP content is subject to the terms at: http://scitation.aip.org/termsconditions. Downloaded to IP: 134.58.253.57 On: Fri, 13 Feb 2015 06:04:46

Direct visualization of boron dopant distribution and coordination in individual chemical vapor deposition nanocrystalline B-doped diamond grains

Ying-Gang Lu,[1] Stuart Turner,[1,a)] Johan Verbeeck,[1] Stoffel D. Janssens,[2,3] Patrick Wagner,[2,3] Ken Haenen,[2,3] and Gustaaf Van Tendeloo[1]
[1]*EMAT, University of Antwerp, Groenenborgerlaan 171, B-2020 Antwerp, Belgium*
[2]*Institute for Materials Research (IMO), Hasselt University, Wetenschapspark 1, B-3950 Diepenbeek, Belgium*
[3]*IMOMEC, IMEC vzw, Wetenschapspark 1, B-3590 Diepenbeek, Belgium*

(Received 22 May 2012; accepted 9 July 2012; published online 25 July 2012)

The boron dopant distribution in individual heavily boron-doped nanocrystalline diamond film grains, with sizes ranging from 100 to 350 nm in diameter, has been studied using a combination of high resolution annular dark field scanning transmission electron microscopy and spatially resolved electron energy-loss spectroscopy. Using these tools, the boron distribution and local boron coordination have been determined. Quantification results reveal embedding of B dopants in the diamond lattice, and a preferential enrichment of boron at defective areas and twin boundaries. Coordination mapping reveals a distinct difference in coordination of the B dopants in "pristine" diamond areas and in defective regions. © *2012 American Institute of Physics*. [http://dx.doi.org/10.1063/1.4738885]

Nanocrystalline diamond (NCD) thin films are widely known for their unique properties such as their wide band gap, extreme hardness, high Young modulus and highest thermal conductivity at room temperature. Doping diamond with boron is a well-established route to control the electrical conductivity of diamond films. However, the local distribution of B within (individual grains of) boron-doped NCD (B:NCD) films has long remained unclear. Huang *et al*. evidenced a depletion of B at grain boundaries in chemical vapor deposition (CVD) grown diamond films,[1] while a clear enrichment of B at grain boundaries and amorphous carbon pockets in polycrystalline high pressure high temperature B: diamond was also evidenced by energy-filtered transmission electron microscopy (TEM).[2] Others suggest a grain size or grain boundary dependence of the B uptake in CVD diamond films.[3] A recent annular dark field scanning transmission electron microscopy (ADF-STEM) investigation by Alegre *et al*.[4] claimed that boron was enriched at grain boundaries of heavily boron-doped microwave plasma CVD diamond and that boron incorporation was nearly constant in all the grains. Our own recent work showed that even though B was present in the amorphous grain boundaries in CVD B:NCD, no clear enrichment of the boron at grain boundaries was apparent.[5] Inside individual diamond grains, the density of extended planar lattice defects has also been shown to be considerably higher in B:NCD diamond films from CVD, an indication that B could well be enriched at planar defects and other defect centers.[6] However, the atomic scale of planar defects, the relatively low B concentration, and problems of specimen preparation for NCD films have strongly hindered the acquisition of detailed experimental data until now.

In this work, we set out to directly visualize the boron dopant distribution and investigate the local boron environment at (planar) defective regions as well as non-defective regions in single B-doped, CVD-grown nanocrystalline diamond grains by means of high resolution ADF-STEM and spatially resolved electron energy-loss spectroscopy (STEM-EELS). Electron energy-loss spectroscopy is ideally suited as the strength of the B-K and C-K edges can be used to map out the elemental distribution of boron and carbon, while the fine structure of the EELS edges can provide insight into the local bonding/coordination of the mapped elements.

B:NCD film growth was carried out in an ASTeX 6500 series microwave plasma enhanced CVD reactor on an electrically insulating fused silica substrate that was treated with a colloidal suspension of 5-10 nm detonation diamond.[7] Growth was performed in a CH_4/H_2 plasma with a methane concentration of 1%. Boron dopants were introduced by trimethyl boron gas ($B(CH_3)_3$) to achieve a nominal 5000 ppm B/C ratio in the gas phase. The substrate temperature of 700 °C was induced by 3500 W of microwave power at a total pressure of 33 hPa (25 torr). The growth was stopped when the B:NCD layers reached a thickness of ~150 nm, after which the sample was cooled down under a hydrogen flow.[8]

A plan-view electron transparent TEM sample was prepared by a combination of mechanical polishing and ion-milling. The sample was cut using a diamond wire and subsequently polished down to micrometer thickness. Further thinning of the sample was performed by ion-milling in a Balzers Ar ion mill, starting with a 12 kV beam until film perforation, continuing with a 5 kV beam for thinning and a 2 kV beam for final polishing.

Electron microscopy was performed on a FEI Titan 80-300 "cubed" microscope fitted with an aberration-corrector for the probe forming lens and a GIF quantum energy filter for spectroscopy, operated at 120 kV to minimize beam damage to the specimen. ADF-STEM imaging was performed using a convergence semi-angle α of ~21 mrad and an ADF inner collection semi-angle of ~27 mrad. The electron probe size at these conditions was approximately 1 Å. STEM-EELS

a)Author to whom correspondenece should be addressed. Electronic mail: stuart.turner@ua.ac.be.

 © 2012 American Institute of Physics

This article is copyrighted as indicated in the article. Reuse of AIP content is subject to the terms at: http://scitation.aip.org/termsconditions. Downloaded to IP: 134.58.253.57 On: Fri, 13 Feb 2015 06:04:46

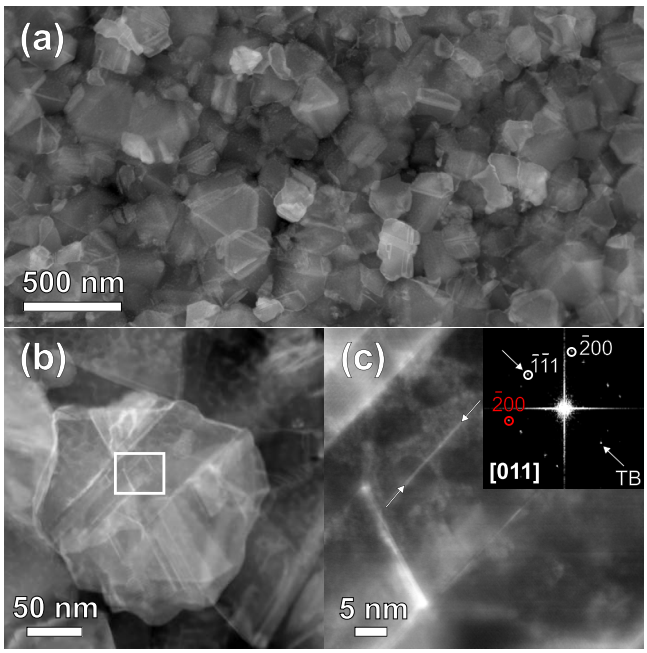

FIG. 1. *ADF-STEM imaging of the investigated B:NCD film in plan-view.* (a) Low magnification ADF-STEM image showing the randomly oriented diamond grains. (b) High magnification ADF-STEM image showing the presence of multiple defects in a single diamond grain. (c) High resolution ADF-STEM image of the region indicated in by the white square in (b). The inset Fourier transform of the defect indicated by the white arrows evidences that the defect is a $\Sigma = 3$ twin boundary.

experiments were performed using the same electron probe and a collection semi-angle β of ~60 mrad. All spectra were acquired at an energy dispersion of 0.25 eV per pixel and an energy resolution of approximately 1.2 eV at full width half maximum. Prior to mapping, the EELS data were treated by principle component analysis to minimize the influence of random noise.[9] Maps were generated by plotting the intensity under the corresponding background-subtracted EELS features in each spectrum of the series. Quantification of the EELS data was performed using Hartree-Slater cross sections in Gatan digital micrograph.

Figure 1 shows three ADF-STEM images of the investigated B:NCD sample. The close packing of the diamond grains is apparent from the plan-view image in Figure 1(a). The diamond grains are easily distinguishable and have sizes ranging from 100 to 350 nm in diameter. Minimal non-sp^3 carbon is present at the grain boundaries, in stark contrast with earlier investigations on micron-sized polycrystalline boron-doped diamond.[2] The inner detection semi-angle of 27 mrad employed for dark-field imaging in these experiments gives rise to an ADF image contrast that is dominated by both mass-thickness and diffraction contrast, making (planar) defects remarkably easy to distinguish.[10,11] Defects are abundant within individual diamond grains, as clearly demonstrated from the ADF image in Figure 1(b). Many studies have already shown that structural imperfections like twins and stacking faults are common features in CVD grown diamond films because of the non-equilibrium nature of the CVD process.[12–14] The dominant defects present in the diamond grains in our sample are $\Sigma = 3$ {111} twin boundaries, which are easily recognizable by the 70.5° or 109.5° angles between the defects, a result of the angle between two {111} planes in the [011] zone axis orientation. Examples of such planar defects are visible in both Figures 1(b) and 1(c). The Fourier transform and high resolution ADF-STEM image of a single defect in Figure 1(c) unequivocally demonstrates the mirror plane to be of the {111} type. $\Sigma = 3$ twin boundaries are known to be the most effective way for the diamond lattice to cope with accumulating strain that results from the incorporation of impurities during film growth.[6,14] Twin boundaries and incoherent defects/regions in diamond are, therefore, a likely position for boron enrichment during growth.

In order to gain insight into how the boron dopants are locally distributed within individual diamond grains (whether the dopants are enriched at defects such as twin boundaries) and what the local coordination of the dopants is at these sites, STEM-EELS measurements were performed on a single diamond grain containing both $\Sigma = 3$ {111} twin boundaries as well as higher order twin boundaries and

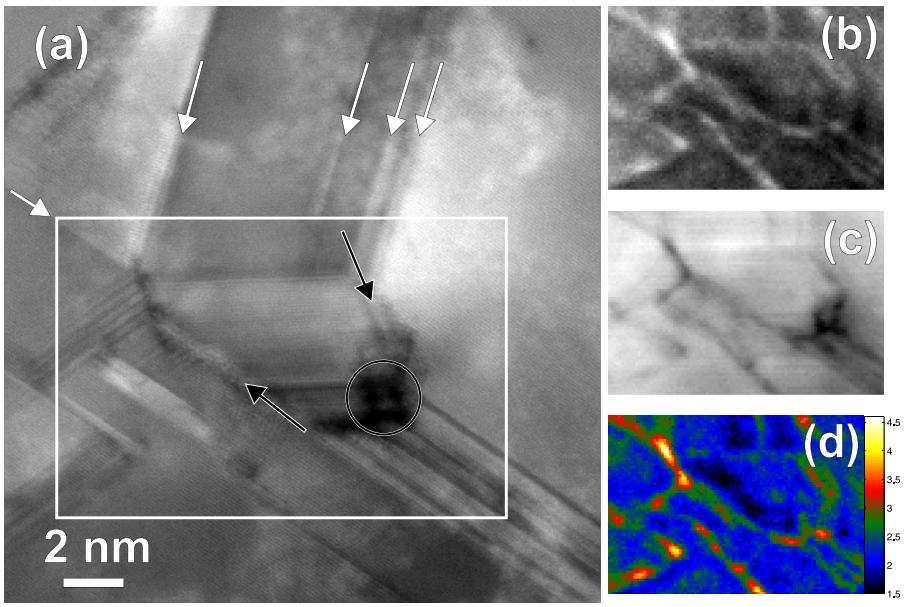

FIG. 2. *Boron and carbon distribution in and around defects in a single diamond grain.* (a) ADF-STEM image of a defect-rich region in a single diamond grain (white arrows: $\Sigma = 3$ twin boundaries, black arrows and black circle: higher order defects and incoherent region). The region used for acquisition of the 102×68 pixel EELS spectrum image is indicated by the white rectangle. (b) B map, (c) C map, (d) B/C ratio map with values ranging from 1.5 to 4.3 at. % B.

This article is copyrighted as indicated in the article. Reuse of AIP content is subject to the terms at: http://scitation.aip.org/termsconditions. Downloaded to IP: 134.58.253.57 On: Fri, 13 Feb 2015 06:04:46

incoherent defect regions. To acquire the spectroscopic data, the so-called spectrum imaging (SI) technique was adopted.[15] In this technique, the Ångström-sized electron probe is scanned over the sample in a raster and an EELS spectrum (in this case containing the B-K and C-K edges) is acquired in each scan point together with the annular dark-field signal.

In Figure 2(a), the region used for acquisition of a 102×68 pixel spectrum image is indicated by the white rectangle. By plotting the intensity under the B-K starting at 188.0 eV and C-K edge starting at 285.0 eV in the EELS spectra of each pixel in the SI, boron and carbon elemental maps have been generated and are plotted in Figures 2(b) and 2(c), respectively. The boron map shows a clear enrichment of B at the $\Sigma = 3$ twin boundaries, the higher order boundaries, and the incoherent regions. The carbon map shows the inverse; the carbon signal is clearly lower at the boundary regions. A quantitative B/C ratio map was generated using Hartree-Slater cross sections and is plotted in Figure 2(d). The boron content in the diamond grains varies from ~1.5 at. % in the perfect diamond regions over ~3 at. % at the $\Sigma = 3$ twin boundaries to a maximum of ~ 4.3 at. % in some of the higher order boundaries and incoherent regions. In summary, the boron in the B:NCD grains is embedded throughout the grains, but preferentially at twin boundaries and incoherent regions.

It is well known that the fine structure of EELS edges, the so-called energy-loss near edge structure or ELNES, is sensitive to the local environment of the excited atom.[16,17] The shape of the ELNES signature of boron and carbon should, therefore, provide information on the local B and C bonding and coordination in the pristine diamond regions and at defects. The ELNES signatures for both boron and carbon from a pristine diamond region and a defect center are plotted in Figures 3(a) and 3(b). The ELNES signature of carbon from the pristine region, dominated by a large σ^* contribution starting from 290.0 eV with three peaks at 292.0, 297.8, and 305.5 eV, is typical for the tetrahedral coordination (sp^3) of carbon in diamond.[15] The small π^* contribution measured at 285.0 eV in the pristine region is indicative of sp^2 hybridized carbon and is most likely due to some amorphous surface carbon. The carbon ELNES from the defected region is similar, yet shows some subtle differences; the π^* contribution at 285.0 eV is higher, most likely

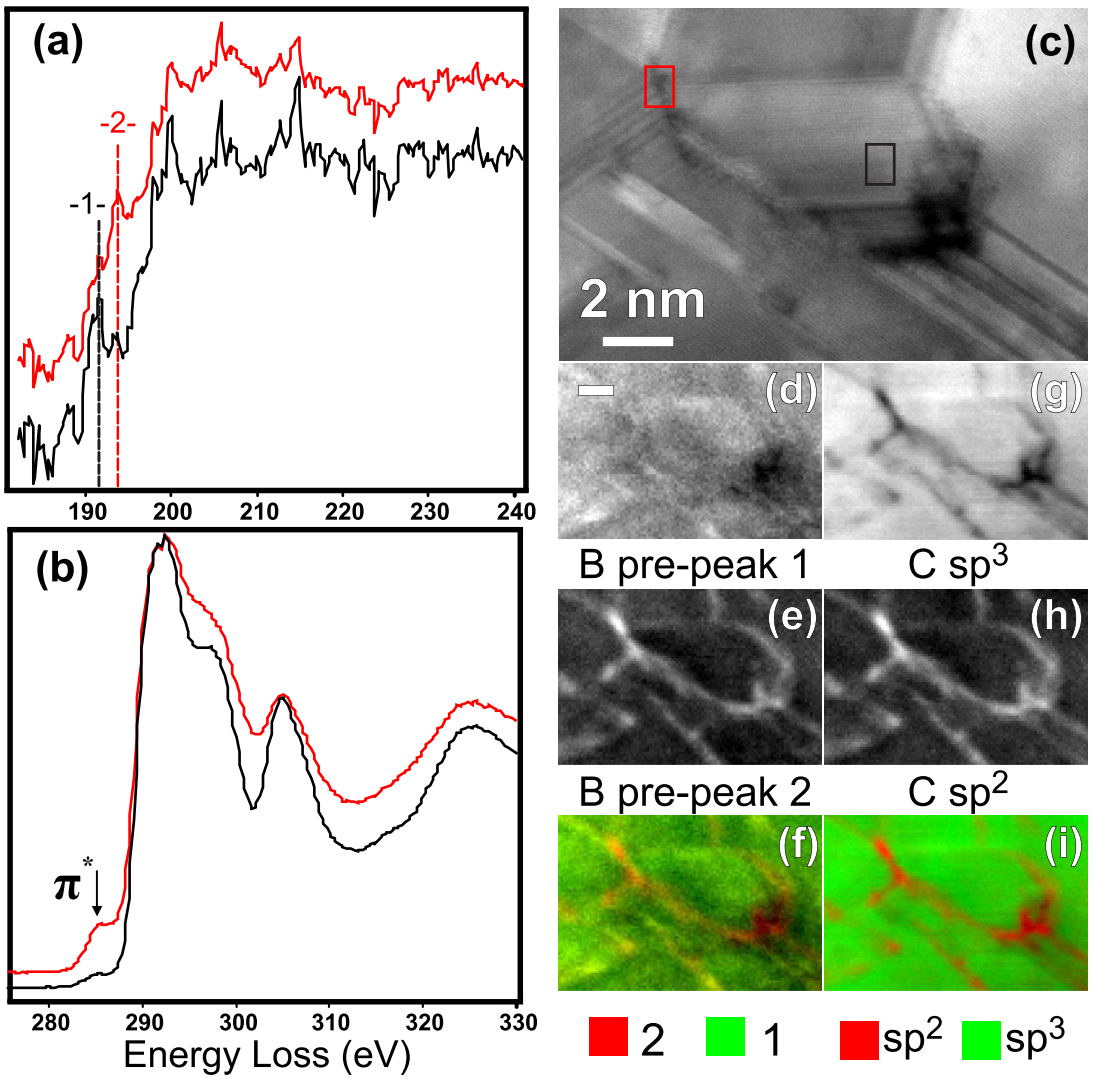

FIG. 3. *Boron and carbon EELS fine structure analysis and coordination mapping*. (a) 20 spectrum summed boron ELNES signatures from a defected (red) and perfect diamond (black) region indicated in (c). (b) Carbon ELNES signatures from the same regions. (c) ADF-STEM image of the SI region. (d) B pre-peak 1 map, (e) B pre-peak 2 map, (f) color map, (g) C sp^3 (σ^*) map, (h) C sp^2 (π^*) map, and (i) color map. The scale bar in image (d) is 2 nm.

This article is copyrighted as indicated in the article. Reuse of AIP content is subject to the terms at: http://scitation.aip.org/termsconditions. Downloaded to IP: 134.58.253.57 On: Fri, 13 Feb 2015 06:04:46

due to the presence of dangling bonds and other sources of non-sp^3 hybridized carbon present in the defect.[18] The peaks in the σ^* region are also less-defined, indicative of small bond length variations in the defective region.[19]

The boron K-edge ELNES from the pristine diamond region is dominated by three peaks centered on 200.0, 205.8, and 214.8 eV. The similarity to the C K-edge ELNES for diamond, dominated by the σ^* contributions at 292.0, 297.8, and 305.5 eV is apparent. This similarity implies that the excited boron atoms are embedded in a similar local environment to the excited carbon atoms. These boron K-edge σ^* features do not fully match with diamond σ^*, which can be explained by the fact that its nearest neighbor atom distances are different than those for carbon in the diamond crystal lattice and by the different electronic structure of B with respect to C. Two small pre-peaks, the first (dominant) pre-peak at ~191.3 eV (labeled -1-) and the second at 193.8 eV (labeled -2-) are also present in the spectrum. In the defective region, the relative intensity of the two pre-peaks is inverted. Pre-peak 1, strongly dominant in the pristine area, is strongly suppressed while pre-peak 2 is enhanced. Similar to the effect in the carbon ELNES, the σ^* contribution in the boron ELNES from the defective region is broadened, showing less definition in the three σ^* peaks. The changing of the relative intensity of the two pre-peaks and literature data provide clues to their origin. First, recent density functional theory (DFT) ELNES calculations for single substitutional B in diamond properly reproduced the three σ^* peaks as well as a small pre-peak 8.7 eV before the first σ^* peak arising from states in the band-gap.[5] This energy position is in excellent agreement with our experimental data for pre-peak 1. Second, literature data from B-doped Fe-Cr oxide reveal a strong π^* signature for B at 193.5, which is again in good agreement with our value of 193.8 eV.[20] Thus, pre-peak 1 is clearly related to a tetrahedral coordination of B in diamond. Pre-peak 2, which is enhanced in the defective region, is related to boron in a trigonal coordination.

Using the fine structure differences in the B and C ELNES signatures, fine structure maps similar to the elemental maps in Figure 2 can be generated. Figure 3(c) once more shows the ADF-STEM image of the SI acquisition region used for elemental mapping in Figure 2. In Figures 3(d)–3(i), the intensity under the specific ELNES features discussed above is used to provide coordination maps for B (pre-peak 1 related to tetrahedrally embedded boron and pre-peak 2 related to trigonal boron) and C (sp^3 and sp^2 carbon). The fine structure maps for boron confirm the link between the two pre-peaks and the boron coordination. The map of the first pre-peak is highly similar to the diamond (C-sp^3) map, meaning that the boron atoms providing this ELNES signature are indeed embedded in the pristine diamond region as substitutional impurities. The darker regions in Figure 3(d), indicative of a lower B pre-peak 1 intensity, clearly correspond to defective areas in the ADF-STEM image. As expected, the pre-peak 2 map (Figure 3(e)) shows a higher intensity at defective regions, confirming that the second pre-peak is indicative of B in a trigonal coordination.

In summary, through use of spatially resolved EELS experiments, we have quantitatively shown the distribution of B dopants within a single, defected diamond grain in a B:NCD film. The results clearly demonstrate the presence of B dopants in the diamond lattice and also an enrichment of these dopants within twin boundaries and defect centers. Using small details in the fine structure of the EELS spectra, chemical bond maps have been generated and we have shown a different coordination of the B dopants embedded within pristine diamond regions and at defective centers and boundaries.

This work was performed within the framework of an IAP P6/42 project of the Belgian government. The authors acknowledge financial support from the Fund for Scientific Research Flanders (FWO) under Contract No. G.0568.10N. The authors acknowledge support from the European Union under a Contract from an Integrated Infrastructure Initiative (Reference 262348 ESMI), the Marie Curie ITN "MATCON" (PITN-GA-2009-238201), and the Collaborative Project "DINAMO" (No. 245122). G.V.T. and J.V. acknowledge the ERC Grant N246791-COUNTATOMS and ERC Starting Grant 278510 VORTEX. S.T. gratefully acknowledges financial support from the FWO. The microscope used in this study was partially financed by the Hercules Foundation of the Flemish Government.

[1]J. T. Huang, C. S. Hu, J. Hwang, H. Chang, and L. J. Lee, Appl. Phys. Lett. **67**(16), 2382 (1995).
[2]N. Dubrovinskaia, R. Wirth, J. Wosnitza, T. Papageorgiou, H. F. Braun, N. Miyajima, and L. Dubrovinsky, Proc. Natl. Acad. Sci. **105**(33), 11619 (2008).
[3]S. Sahli and D. M. Aslam, Appl. Phys. Lett. **70**(16), 2129 (1997).
[4]M. P. Alegre, M. P. Villar, D. Araujo, E. Bustarret, T. Capron, and O. A. Williams, AIP Conf. Proc. **1292**(1), 133 (2010).
[5]S. Turner, Y. Lu, S. Janssens, F. Da Pieve, D. Lamoen, J. Verbeeck, K. Haenen, P. Wagner, and G. Van Tendeloo, "Local Boron Environment in B-doped Nanocrystalline Diamond Films," Nanoscale (submitted).
[6]J. W. Steeds, A. E. Mora, J. E. Butler, and K. M. Bussmann, Philos. Mag. A **82**(9), 1741 (2002).
[7]O. A. Williams, O. Douhéret, M. Daenen, K. Haenen, E. Osawa, and M. Takahashi, Chem. Phys. Lett. **445**(4–6), 255 (2007).
[8]S. D. Janssens, P. Pobedinskas, J. Vacik, V. Petráková, B. Ruttens, J. D'Haen, M. Nesládek, K. Haenen, and P. Wagner, New J. Phys. **13**(8), 083008 (2011).
[9]P. Trebbia and N. Bonnet, Ultramicroscopy **34**(3), 165 (1990).
[10]H. Idrissi, S. Turner, M. Mitsuhara, B. Wang, S. Hata, M. Coulombier, J.-P. Raskin, T. Pardoen, G. Van Tendeloo, and D. Schryvers, Microsc. Microanal. **17**, 983 (2011).
[11]R. Erni, B. Freitag, P. Hartel, H. Müller, P. Tiemeijer, M. van der Stam, M. Stekelenburg, D. Hubert, P. Specht, and V. Garibay-Febles, Microsc. Microanal. **12**, 492 (2006).
[12]W. Zhu, A. R. Badzian, and R. Messier, J. Mater. Res. **4**, 659 (1989).
[13]D. Shechtman, J. L. Hutchison, L. H. Robins, E. N. Farabaugh, and A. Feldman, J. Mater. Res. **8**, 473 (1993).
[14]D. Shechtman, A. Feldman, and J. Hutchison, Mater. Lett. **17**(5), 211 (1993).
[15]R. F. Egerton, *Electron Energy-Loss Spectroscopy in the Electron Microscope* (3rd Edition) (Springer, New York, 2011).
[16]L. A. J. Garvie, A. J. Craven, and R. Brydson, Am. Mineral. **80**(11–12), 1132 (1995).
[17]L. A. J. Garvie, H. Hubert, W. T. Petuskey, P. F. McMillan, and P. R. Buseck, J. Solid State Chem. **133**(2), 365 (1997).
[18]S. Turner, O. Shenderova, F. Da Pieva, E. Yücelen, D. Lamoen, and G. Van Tendeloo, "Aberration-corrected microscopy and spectroscopy analysis of pristine, nitrogen containing detonation nanodiamond," (submitted).
[19]J. T. Titantah and D. Lamoen, Phys. Rev. B **72**(19), 193104 (2005).
[20]H. Sauer, R. Brydson, P. N. Rowley, W. Engel, and J. M. Thomas, Ultramicroscopy **49**(1–4), 198 (1993).

This article is copyrighted as indicated in the article. Reuse of AIP content is subject to the terms at: http://scitation.aip.org/termsconditions. Downloaded to IP: 134.58.253.57 On: Fri, 13 Feb 2015 06:04:46